

## Superconductive materials with MgB<sub>2</sub>-like structures from data-driven screening

Ze Yu <sup>1,2,\*</sup> Tao Bo<sup>1,3,\*</sup> Bo Liu<sup>1,2</sup> Zhendong Fu,<sup>3</sup> Huan Wang,<sup>4,5</sup> Sheng Xu,<sup>4,5</sup>  
Tianlong Xia <sup>4,5,†</sup> Shiliang Li,<sup>1,2,3,‡</sup> Sheng Meng,<sup>1,2,3,§</sup> and Miao Liu <sup>1,3,6,||</sup>

<sup>1</sup>Beijing National Laboratory for Condensed Matter Physics, Institute of Physics, Chinese Academy of Sciences, Beijing 100190, China

<sup>2</sup>School of Physical Sciences, University of Chinese Academy of Sciences, Beijing 100190, China

<sup>3</sup>Songshan Lake Materials Laboratory, Dongguan, Guangdong 523808, China

<sup>4</sup>Department of Physics, Renmin University of China, Beijing 100872, China

<sup>5</sup>Beijing Key Laboratory of Opto-electronic Functional Materials & Micro-nano Devices, Renmin University of China, Beijing 100872, China

<sup>6</sup>Center of Materials Science and Optoelectronics Engineering, University of Chinese Academy of Sciences, Beijing 100049, China



(Received 24 February 2022; accepted 7 June 2022; published 22 June 2022)

Finding viable superconducting materials is of interest to the physics community, as the superconductors are the playground for manifesting many appealing quantum phenomena. In this paper, we exemplify an end-to-end materials discovery toward MgB<sub>2</sub>-like superconductors, starting from data-driven compound screening to experimental materialization. In addition to the known superconducting compounds, CaB<sub>2</sub> ( $T_c = 9.4\text{--}28.6\text{ K}$ ), SrGa<sub>2</sub> ( $T_c = 0.1\text{--}2.4\text{ K}$ ), BaGa<sub>2</sub> ( $T_c = 0.3\text{--}3.3\text{ K}$ ), BaAu<sub>2</sub> ( $T_c = 0.0\text{--}0.5\text{ K}$ ), and LaCu<sub>2</sub> ( $T_c = 0.1\text{--}2.2\text{ K}$ ) are discovered, out of  $\sim 182\,000$  starting structures, to be the most promising superconducting compounds that share similar atomic structures with MgB<sub>2</sub>. Moreover, BaGa<sub>2</sub> is experimentally synthesized and measured to confirm that the compound is a Bardeen-Cooper-Schrieffer superconductor with  $T_c = 0.36\text{ K}$ , in good agreement with our theoretical predictions. In this paper, we provide a study for the MgB<sub>2</sub>-like superconductors and showcase that it is feasible to discover materials via a data-driven approach.

DOI: [10.1103/PhysRevB.105.214517](https://doi.org/10.1103/PhysRevB.105.214517)

### I. INTRODUCTION

Superconductivity is a fascinating and robust quantum phenomenon to manifest the many-body correlations in solids. It was discovered by Onnes [1] that mercury became superconductive  $< 4.2\text{ K}$ , and then various superconducting materials have been found to have elevated  $T_c$ , including niobium-germanium alloy ( $T_c = 23.2\text{ K}$ ) [2], lanthanum barium copper oxide ( $T_c = 35.0\text{ K}$ ) [3], MgB<sub>2</sub> ( $T_c = 39.0\text{ K}$ ) [4], yttrium barium copper oxide ( $T_c = 92.0\text{ K}$ ) [5], pressured H<sub>3</sub>S ( $T_c = 203.5\text{ K}$ ) [6], and recently, carbonaceous sulfur hydride under pressure ( $T_c = 287.7\text{ K}$ ) [7]. Among those systems, MgB<sub>2</sub> possesses superior properties, warranting its great potential for various applications [8]. For example, the high  $T_c$  enables the operation of the MgB<sub>2</sub> circuits  $> 20\text{ K}$ , which is higher than the operating temperature of Nb-based superconducting electronics [9]. In addition, MgB<sub>2</sub> can survive under a higher magnetic field than that of Nb-based superconductors; therefore, MgB<sub>2</sub> can be utilized as the magnet material in cryogen-free magnetic resonance imaging (MRI) devices [10–14]. Given the appealing advantages of MgB<sub>2</sub>, it would be of great interest for the superconductor community to thoroughly screen and evaluate the superconductivity within the MgB<sub>2</sub>-like structures.

Taking advantage of recent progress on materials databases, in this paper, we obtain 56 compounds in total that share the same MgB<sub>2</sub>-like crystal structure after intensive structural screening, which started from  $\sim 180\,000$  inorganic compounds from Atomly [15]. Further screening based on thermodynamic stability as well as dynamic stability narrows down the possibility to only 26 compounds. Since MgB<sub>2</sub> was confirmed to satisfy the Bardeen-Cooper-Schrieffer (BCS) theory, the coupling of the electrons to lattice vibrations can be fairly accurately addressed via first-principles calculations. Hence, all 26 candidates are fed into the following superconducting evaluation at the first-principles level. It is found that the XB<sub>2</sub> ( $X = \text{Mg, Al, Ca, Sc, V, Y, Nb, and Ta}$ ), XSi<sub>2</sub> ( $X = \text{Ca}$ ), XGa<sub>2</sub> ( $X = \text{Sr and Ba}$ ), BaAu<sub>2</sub>, and LaCu<sub>2</sub> are superconductive. To validate our approach, one of these compounds, BaGa<sub>2</sub>, has been experimentally made and tested to confirm that the BaGa<sub>2</sub> compound is indeed a superconductor with  $T_c = 0.36\text{ K}$ , in very good agreement with our predictions based on *ab initio* calculations. In this paper, we demonstrate that the BCS superconductors can be discovered in a fairly cost-effective manner through high-throughput computations, and we also provide the superconductor community with a viable phase space to search for feasible MgB<sub>2</sub>-like superconductors.

### II. COMPUTATION DETAILS

The materials data used in this paper are obtained from Atomly [15], open-access density functional theory materials data infrastructure which is conceptually like the Materials Project [16], AFLOWlib [17], and OQMD [18]. The data

\*These authors contributed equally to this paper.

†txia@ruc.edu.cn

‡slli@iphy.ac.cn

§smeng@iphy.ac.cn

||mliu@iphy.ac.cn

are generated through high-throughput first-principles calculations with an automated workflow to crunch through >180 000 inorganic crystal materials. The dataset contains the crystal structure [e.g., crystal structure, x-ray diffraction], electronic structure [e.g., the density of states and bandgap ( $E_g$ )], and energies [e.g., formation energy ( $E_{\text{form}}$ ), energy above the convex hull ( $E_{\text{hull}}$ )] of the compounds, basically all the properties which can be obtained from first-principles calculation. The data are calculated by using the Vienna *Ab initio* Simulation Package (VASP) [19] and the Perdew-Burke-Ernzerhof [20] exchange-correlation functional of generalized gradient approximation to deal with the interactions between electrons. The cutoff energy for plane waves is 520 eV, and the k-mesh is  $3000/\text{\AA}^3$  or higher.

After the screening, structural optimization is performed for all candidate materials. The plane-wave cutoff was set to be 520 eV with a k-point mesh of  $(17 \times 17 \times 15)$  in the Monkhorst-Pack sampling scheme. For geometric optimization, all atoms are allowed to fully relax until the forces on atoms are  $< 0.01 \text{ eV/\AA}$ , after considering spin polarization.

The phonon dispersion, electron-phonon coupling (EPC), and superconducting properties are performed using the QUANTUM ESPRESSO package [21]. The plane-wave kinetic-energy cutoff and the energy cutoff for charge density are set as 100 and 800 Ry, respectively. The Brillouin zone (BZ) k-point mesh of  $24 \times 24 \times 24$  and a Methfessel-Paxton smearing width of 0.02 Ry are used to calculate the self-consistent electron density. The dynamic and EPC matrix elements are computed within an  $8 \times 8 \times 8$  q mesh. The phonon properties and EPC are calculated based on the density functional perturbation (DFPT) [22] and Eliashberg theories [23]. The calculation details are shown in the Supplemental Material [24] (see also Refs. [25–28] therein).

Single crystals of  $\text{BaGa}_2$  were grown by the self-flux method, as reported previously [29]. The resistivity, magnetic susceptibility, and specific heat were measured on a physical property measurement system (Quantum Design) with the dilution refrigerator insert.

### III. RESULTS AND DISCUSSIONS

To comprehensively screen the  $\text{MgB}_2$ -like materials from the database, the  $\text{MgB}_2$  structure (space group  $P6/mmm$ , ICSD ID 193379, Materials Project ID mp-763, and Atomly ID 0000105522) is used as the structural template. There are two planar layers of atoms in each primitive cell: the metallic element ( $X$ ) forms a triangle lattice layer, and the nonmetallic element ( $Y$ ) forms the honeycomb lattice layer; and the two planar layers repeat themselves in the  $c$  direction alternatively, forming the stoichiometry of  $XY_2$ , as shown in Fig. 1(a).

A screening process, as shown in Fig. 1(b), is performed on a dataset of the 182 155 material structures, which is obtained from the Atomly database, to filter out all the compounds with  $\text{MgB}_2$  geometry. An in-house script along with the Structure-Matcher module of the pymatgen library [30] is employed to extract all the compounds with the  $\text{MgB}_2$ -like structure, and all radioactive-element-containing compounds are excluded. After the rigorous filtration process, 56 compounds fall out to have the  $\text{MgB}_2$ -like structure. Then the following screening on the thermodynamic stability narrows down the candidate

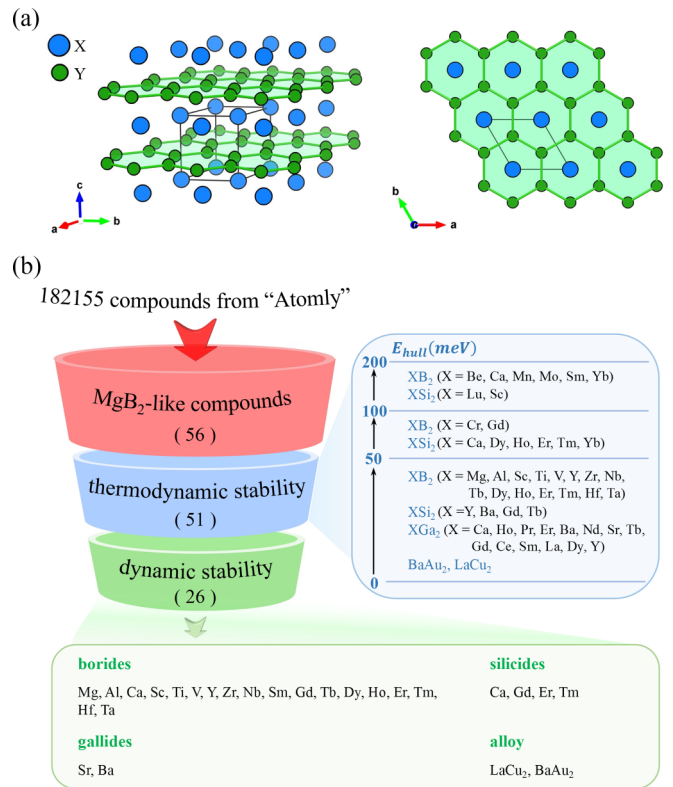


FIG. 1. (a) The side and top view of the  $\text{MgB}_2$ -like materials. (b) The screening flow chart for  $\text{MgB}_2$ -like materials. The total process is divided into three steps: filtering out all  $\text{MgB}_2$ -like materials and evaluating thermodynamic stability and dynamics stability. The thermodynamically stable materials are summarized in the table on the right, while the dynamically stable ones are summarized in the table below.

materials to 51 compounds. The thermodynamic stability of the compounds is assessed by the physical quantity of energy above hull ( $E_{\text{hull}}$ ), which is the reaction enthalpy required to decompose a material to other stable compounds. The detailed definition of  $E_{\text{hull}}$  can be found in Refs. [31,32]. Thermodynamically wise, a compound with  $E_{\text{hull}} = 0 \text{ meV/atom}$  is the most stable compound, and the stability is worsening when  $E_{\text{hull}}$  increases. Out of the 56 candidates,  $E_{\text{hull}}$  of 51 structures are  $< 200 \text{ meV/atom}$ , 43 structures are  $< 100 \text{ meV/atom}$ , and 35 structures are  $< 50 \text{ meV/atom}$ . Normally, the threshold of  $200 \text{ meV/atom}$  is a good value to indicate that the compound is likely to be synthesized, and  $50 \text{ meV/atom}$  means the compound is highly likely to be synthesized [33,34]. Finally, the dynamic stability assessment based on phonon spectrum calculations shows that there are 26 dynamically stable materials. They are  $\text{MgB}_2, \text{AlB}_2, \text{CaB}_2, \text{ScB}_2, \text{TiB}_2, \text{VB}_2, \text{YB}_2, \text{ZrB}_2, \text{NbB}_2, \text{SmB}_2, \text{GdB}_2, \text{TbB}_2, \text{DyB}_2, \text{HoB}_2, \text{ErB}_2, \text{TmB}_2, \text{HfB}_2, \text{TaB}_2, \text{CaSi}_2, \text{GdSi}_2, \text{ErSi}_2, \text{TmSi}_2, \text{SrGa}_2, \text{BaGa}_2, \text{BaAu}_2, \text{and LaCu}_2$  (see Figs. S1–S4 in the Supplemental Material [24]). Other compounds,  $\text{BeB}_2, \text{CrB}_2$ , etc., are found to be dynamically unstable due to the presence of imaginary frequencies in their phonon spectrum. According to the species of anions, these 26 materials can be divided into four categories: the borides  $\text{XB}_2$  ( $X = \text{Mg, Al, Ca, Sc, Ti, V, Y, Zr, Nb, Sm, Gd, Tb, Dy, Ho, Er, Tm, Hf, and Ta}$ ), the silicides

TABLE I. The total EPC  $\lambda$ ,  $T_c^{\text{cal}}$  by the *ab initio* calculations,  $T_c^{\text{exp}}$  measured by experiments, and corresponding references. The empirical parameter  $\mu^*$  that represents the effective screened Coulomb repulsion for BCS systems is usually system dependent and falls into the  $0.04 < \mu^* < 0.18$  range [56–58]; hence, we derived the upper and lower boundaries of  $T_c$  accordingly.

Formula	$\lambda$	$T_c^{\text{cal}}$ (K)	$T_c^{\text{exp}}$ (K)	Reference
MgB <sub>2</sub>	0.68	10.3–37.9	39.0	[4]
AlB <sub>2</sub>	0.47	0.6–10.9	0.0	[64]
CaB <sub>2</sub>	0.75	9.4–28.6		
ScB <sub>2</sub>	0.28	0.0–1.7	1.5	[65,66]
TiB <sub>2</sub>	0.13	0.0–0.0	0.0	[46]
VB <sub>2</sub>	0.36	0.0–4.2	0.0	[46]
YB <sub>2</sub>	0.40	0.1–6.1	0.0	[67]
ZrB <sub>2</sub>	0.14	0.0–0.0	0.0/5.5	[35,46]
NbB <sub>2</sub>	0.71	5.7–19.4	0.6–9.2	[46–52]
SmB <sub>2</sub>	0.08	0.0–0.0	0.0	[55]
GdB <sub>2</sub>	0.15	0.0–0.0	0.0	[55]
TbB <sub>2</sub>	0.12	0.0–0.0	0.0	[55]
DyB <sub>2</sub>	0.11	0.0–0.0	0.0	[55]
HoB <sub>2</sub>	0.10	0.0–0.0	0.0	[55]
ErB <sub>2</sub>	0.09	0.0–0.0	0.0	[55]
TmB <sub>2</sub>	0.10	0.0–0.0	0.0	[55]
HfB <sub>2</sub>	0.14	0.0–0.0	0.0	[46]
TaB <sub>2</sub>	0.95	9.4–20.3	0.0/9.5	[39,46,53]
CaSi <sub>2</sub>	1.13	8.7–16.0	14.0	[54]
GdSi <sub>2</sub>	0.07	0.0–0.0		
ErSi <sub>2</sub>	0.09	0.0–0.0		
TmSi <sub>2</sub>	0.12	0.0–0.0		
SrGa <sub>2</sub>	0.44	0.1–2.4		
BaGa <sub>2</sub>	0.56	0.3–3.3		
BaAu <sub>2</sub>	0.34	0.0–0.5		
LaCu <sub>2</sub>	0.46	0.1–2.2		

$X\text{Si}_2$  ( $X = \text{Ca}, \text{Gd}, \text{Er}, \text{and Tm}$ ), the gallides  $X\text{Ga}_2$  ( $X = \text{Sr}$  and  $\text{Ba}$ ), and the alloys ( $\text{BaAu}_2$  and  $\text{LaCu}_2$ ).

According to the existing literature, some of these materials have been extensively studied previously [35–45]. For example, MgB<sub>2</sub> and NbB<sub>2</sub> have been found to transition to a superconducting state <39.0 and 9.2 K, respectively. Since MgB<sub>2</sub> belongs to the category of conventional superconductors where BCS theory applies, the EPC as well as the superconducting transition temperature  $T_c$  can be obtained from first-principles calculations.

For the 26 dynamic stable candidates, the EPC constant  $\lambda$  and superconducting transition temperature  $T_c$  are obtained from DFPT calculations, as summarized in Table I. MgB<sub>2</sub> has the highest calculated  $T_c$  of 37.9 K when the empirical parameter  $\mu^*$ , which represents the effective screened Coulomb repulsion, is 0.04, which is in good agreement with  $T_c = 39$  K obtained in the experiment while tolerating computation errors. Previously, it was found in experiments that VB<sub>2</sub>, TiB<sub>2</sub>, and HfB<sub>2</sub> [46] are nonsuperconductive, in good agreement with our prediction. It was also found that ZrB<sub>2</sub> [35,46], NbB<sub>2</sub> [46–52], and TaB<sub>2</sub> [39,46,53] are superconductive with  $T_c$  up to 5.5, 9.2, and 9.5 K, respectively, confirming our predictions too. In those experiments,  $T_c$  is highly tunable by the nonstoichiometric ratio, external impu-

rities, etc.; hence, the experimental values of  $T_c$  may still need further investigation. CaSi<sub>2</sub> has a  $T_c$  of 14 K when it is under high pressure [54], in line with our predicted value, which is  $T_c = 8.7$ –16.0 K. The rare-earth-containing compounds, especially lanthanides (SmB<sub>2</sub>, GdB<sub>2</sub>, TbB<sub>2</sub>, DyB<sub>2</sub>, HoB<sub>2</sub>, ErB<sub>2</sub>, TmB<sub>2</sub>, HfB<sub>2</sub>, GdSi<sub>2</sub>, ErSi<sub>2</sub>, and TmSi<sub>2</sub>), are not superconductors based on our *ab initio* calculations, confirming the experimental data [55]. AlB<sub>2</sub> and YB<sub>2</sub> are two exceptions, as they are superconductive according to our calculations, but nonsuperconductive from real-world experiments; therefore, they are worthy of in-depth studies.

Other than the compounds mentioned above, in this paper, we add CaB<sub>2</sub>, SrGa<sub>2</sub>, BaGa<sub>2</sub>, BaAu<sub>2</sub>, and LaCu<sub>2</sub> to the list of compounds within the MgB<sub>2</sub>-structural family, as they have not yet been experimentally examined. Based on our theoretical evaluation, CaB<sub>2</sub>, SrGa<sub>2</sub>, BaGa<sub>2</sub>, BaAu<sub>2</sub>, and LaCu<sub>2</sub> are highly likely to be superconductive, whereas GdSi<sub>2</sub>, ErSi<sub>2</sub>, and TmSi<sub>2</sub> are nonsuperconductive. The  $T_c$  for CaB<sub>2</sub>, SrGa<sub>2</sub>, BaGa<sub>2</sub>, BaAu<sub>2</sub>, and LaCu<sub>2</sub> are 9.4–28.6 K, 0.1–2.4 K, 0.3–3.3 K, 0.0–0.5 K, and 0.1–2.2 K, respectively. Recently, theoretical work also found that the superconducting transition temperature  $T_c$  of BaGa<sub>2</sub> is 1.2 K [56].

To investigate the EPC and superconducting transition temperature  $T_c$  of CaB<sub>2</sub>, SrGa<sub>2</sub>, and BaGa<sub>2</sub>, we calculate their phonon dispersion, the phononic density of states, Eliashberg spectral function  $\alpha^2F(\omega)$ , and cumulative frequency-dependent EPC constant  $\lambda(\omega)$ , as presented in Fig. 2. In addition to this, the band structures and Fermi surfaces are calculated (see Fig. S5 in the Supplemental Material [24]). For CaB<sub>2</sub>, the Ca vibrations mainly dominate the low frequencies of 0–300 cm<sup>-1</sup>, while the B vibrations mainly dominate the high frequencies >300 cm<sup>-1</sup> [see Figs. 2(a) and 2(c)]. There are some softened phonon modes along the  $\Gamma$ -A line and around the  $\Gamma$  point at  $\sim 350$  cm<sup>-1</sup>, which are associated with the B<sub>xy</sub> vibration, yielding a large EPC  $\lambda_{qv}$ , as shown in Fig. 2(b). The phonon dispersion in the frequency range of 300–600 cm<sup>-1</sup> contributes most to the EPC  $\lambda_{qv}$  [see Fig. 2(d)]. The calculated EPC  $\lambda(\omega)$  of CaB<sub>2</sub> is 0.75, and  $T_c$  is 9.4–28.6 K when  $\mu^*$  is in the 0.04–0.18 range [56–58], which is quite high in this series of materials.

In SrGa<sub>2</sub> and BaGa<sub>2</sub>, some physical properties such as vibration dominance are quite different. For SrGa<sub>2</sub>, the Sr vibrations mainly dominate the low frequencies of 0–120 cm<sup>-1</sup>, while the Ga vibrations spread in the whole area of the BZ [see Figs. 2(e) and 2(f)]. There is a softened phonon mode around the A point, associated with the Ga<sub>z</sub> vibration ( $\sim 40$  cm<sup>-1</sup>), yielding a large EPC  $\lambda_{qv}$ , as shown in Fig. 2(f). In addition, the phonon dispersion in the frequency range of 40–120 cm<sup>-1</sup> contributes most to the EPC  $\lambda_{qv}$ . The calculated EPC  $\lambda(\omega)$  and  $T_c$  for SrGa<sub>2</sub> are 0.44 and 0.1–2.4 K, respectively. The low-frequency phonons (40–120 cm<sup>-1</sup>) contribute 86% of the EPC  $\lambda$ , while the high-frequency phonons (180–220 cm<sup>-1</sup>) contribute  $\sim 14\%$  [see Fig. 2(h)]. The EPC properties of BaGa<sub>2</sub> are roughly the same as SrGa<sub>2</sub> but relatively stronger. As shown in Figs. 2(i) and 2(j), the Ba vibrations mainly dominate the low frequencies of 0–100 cm<sup>-1</sup>, while the Ga vibrations spread in the whole area of the BZ. No imaginary phonon modes indicate that it is dynamically stable, at least from the perspective of the *ab initio* calculations. As shown in

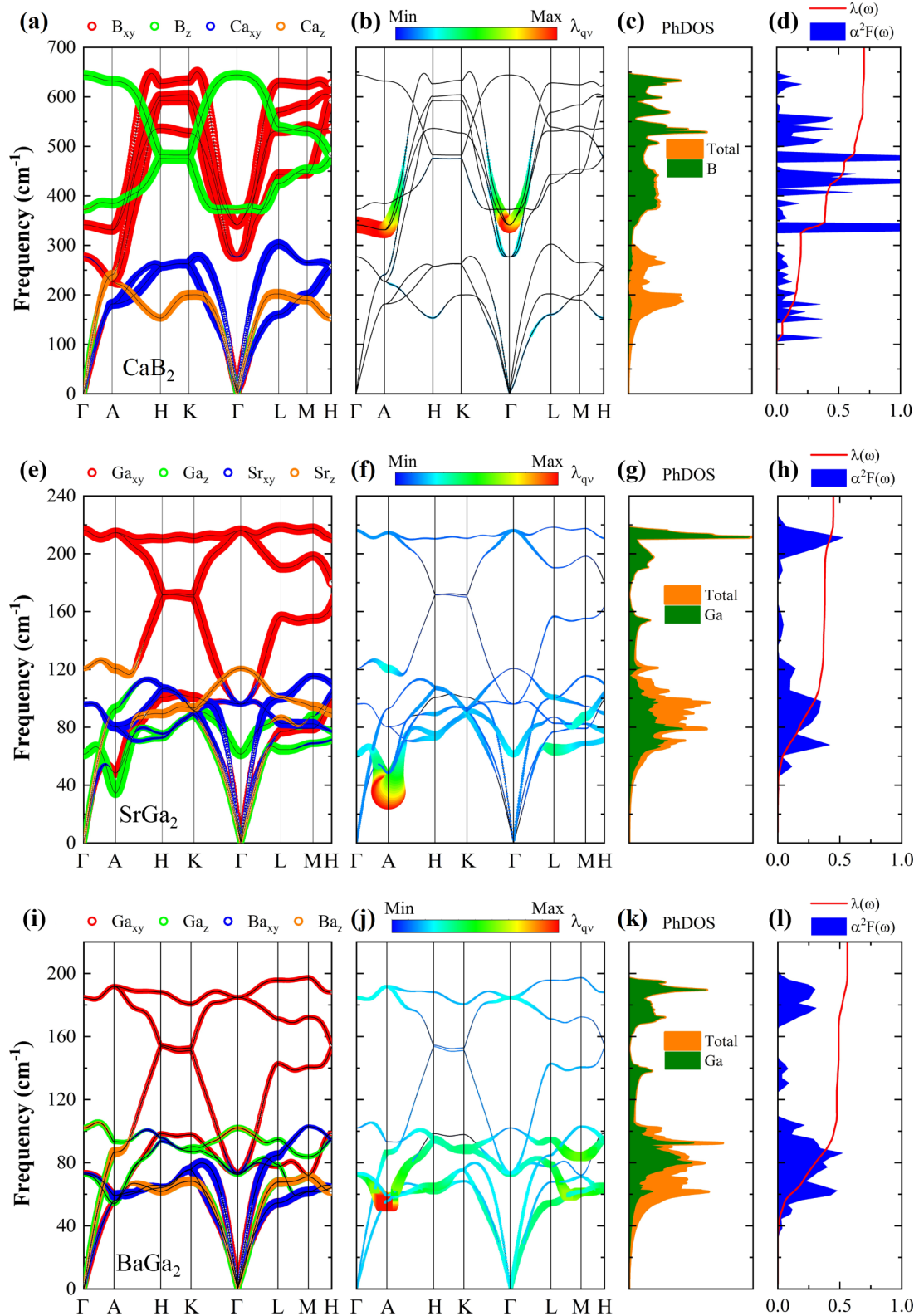


FIG. 2. The phonon dispersion weighted by motion modes of constituent elements, the phonon dispersion weighted by the magnitude of electron-phonon coupling (EPC)  $\lambda_{qv}$ , phononic density of states (PhDOS), Eliashberg spectral function  $\alpha^2F(\omega)$ , and cumulative frequency-dependent of the EPC constant  $\lambda(\omega)$  of (a)–(d) CaB<sub>2</sub>, (e)–(h) SrGa<sub>2</sub>, and (i)–(l) BaGa<sub>2</sub>. The red, green, blue, and orange colors in (a), (e), and (i) represent  $B_{xy}$  ( $Ga_{xy}$ ,  $Ga_{xy}$ ),  $B_z$  ( $Ga_z$ ,  $Ga_z$ ),  $Ca_{xy}$  ( $Sr_{xy}$ ,  $Ba_{xy}$ ), and  $Ca_z$  ( $Sr_z$ ,  $Ba_z$ ) modes, respectively.

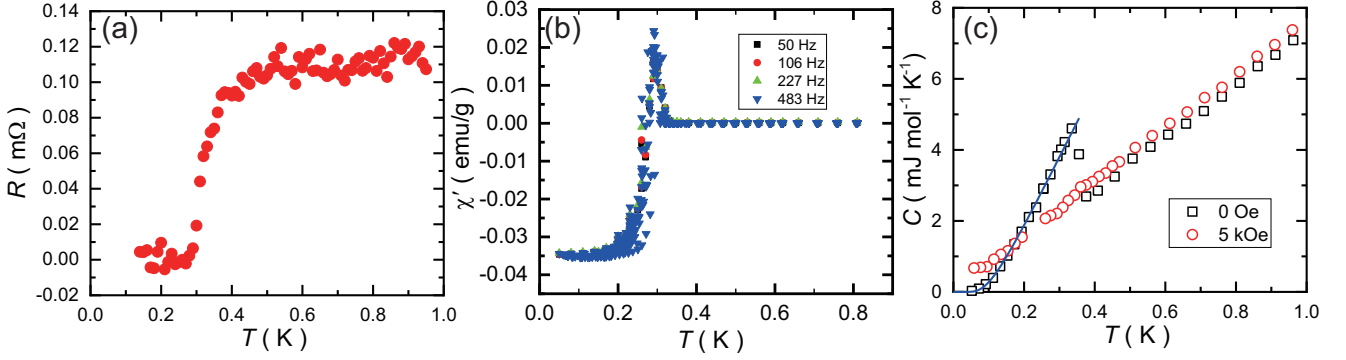


FIG. 3. (a) Temperature dependence of the resistivity. Due to the very small resistance, a current of 0.3 mA was used. (b) Temperature dependence of the real component of the AC susceptibility. (c) Temperature dependence of the specific heat at various fields. The solid line is fitted by Eq. (1).

Figs. 2(j) and 2(l), the low-frequency phonons (40–100 cm<sup>-1</sup>) have a large contribution to the EPC  $\lambda_{qv}$  and total EPC  $\lambda$ . The calculated EPC  $\lambda(\omega)$  and  $T_c$  are 0.56 and 0.3–3.3 K, a little lower than those in CaB<sub>2</sub> and SrGa<sub>2</sub>.

The superconductivity in MgB<sub>2</sub> stems from a strong anisotropic EPC where a large part of the EPC is concentrated in a few lattice modes close to the  $\Gamma$  point [59–62]. Figure 2 shows  $T_c$  is indeed anisotropy dependent. The CaB<sub>2</sub> shows a strong anisotropic EPC, the same as in MgB<sub>2</sub>; hence, it can host the hot phonons without spreading into all other phonon modes. The phonon modes in SrCa<sub>2</sub> and BaGa<sub>2</sub> are less anisotropic than that of MgB<sub>2</sub> and hence lower  $T_c$ .

To validate the high-throughput data-driven prediction based on first principles, the BaGa<sub>2</sub> compound is experimentally synthesized and characterized for its superconductivity. We found that BaGa<sub>2</sub> is indeed a superconductor with a measured  $T_c = 0.36$  K, in good agreement with the theoretical prediction, which is 0.3–3.3 K. The superconducting properties were measured by resistivity, magnetic-susceptibility, and heat-capacity measurements. Figure 3(a) shows the temperature dependence of the resistance, which gives the onset  $T_c$  of  $\sim 0.37$  K. Zero resistance is found  $< 0.29$  K. Figure 3(b) shows the real component of the AC susceptibility  $\chi'$  as the function of temperature, which exhibits the Meissner effect  $< 0.32$  K. Figure 3(c) further shows the temperature dependence of the specific heat. Above 0.4 K, the specific heat is linearly dependent on the temperature, demonstrating that the phonon contribution can be neglected  $< 1$  K. A superconducting jump is found at 0.34 K and disappears  $< 5$  kOe. The behavior below  $T_c$  can be well fitted by the BCS expression for the specific heat:

$$C = \frac{T}{T_c} \frac{d}{dt} \int_0^\infty dy \left( -\frac{6\gamma\Delta_0}{k_B\pi} \right) [f \ln f + (1-f) \ln(1-f)], \quad (1)$$

where  $\gamma$  is the normal-state Sommerfeld coefficient,  $f$  is the Fermi-Dirac distribution function, and  $f = 1/[\exp(E/k_B T) + 1]$ . The energy of quasiparticles is given by  $E = \sqrt{\epsilon^2 + \Delta^2}$ , where  $\epsilon$  is the energy of the normal electrons relative to the Fermi surface. The integration variable is  $y = \epsilon/\Delta$ . Unlike MgB<sub>2</sub> [63], there is no need to introduce two gaps to describe the specific heat data. The fitted value of  $\Delta_0$ ,

the superconducting gap at 0 K, is 0.0433 meV, which gives  $2\Delta_0/k_B T_c = 2.83$  with  $T_c = 0.355$  K.

CaB<sub>2</sub>, which is predicted to have higher  $T_c$ , has moderate thermal stability as  $E_{\text{hull}} = 191$  meV/atom; hence, it is harder to be synthesized via the traditional route. Sometimes soft chemistry, template epitaxial growth, or high-pressure synthesis may be able to overcome the unfavorable phase competition. Combining all the information obtained here, SrGa<sub>2</sub>, BaAu<sub>2</sub>, LaCu<sub>2</sub>, and CaB<sub>2</sub> are worth further experimental explorations.

Some fundable ideas may soar from here: (a) In this paper, we provided a larger chemical space to investigate the trends in MgB<sub>2</sub>-like systems, e.g., the strong anisotropic EPC [59–62] vs  $T_c$ ; (b) BaGa<sub>2</sub> can serve as a viable system to study the interplay between Dirac fermions and superconductivity, as BaGa<sub>2</sub> is a multilayered Dirac semimetal with its quasi-2D Dirac cone located at the Fermi level [29]; and (c) it is suggested to synthesize CaB<sub>2</sub> experimentally under special conditions, such as high pressure, to overcome the moderate thermodynamic instability ( $\sim 190$  meV/atom).

#### IV. CONCLUSIONS

The vast phase space of the MgB<sub>2</sub>-like structures is thoroughly explored to discover superconductive compounds, leveraging the recent advances in high-throughput computing, materials databases, first-principles calculations as well as state-of-art experiments. In this paper, we find that SrGa<sub>2</sub>, BaGa<sub>2</sub>, BaAu<sub>2</sub>, and LaCu<sub>2</sub> are promising superconductors, falling out of  $\sim 182000$  starting structures and of which BaGa<sub>2</sub> is experimentally synthesized and measured to confirm that the compound is a BCS superconductor with  $T_c = 0.36$  K, in line with theoretical predictions. CaB<sub>2</sub> is predicted to have higher  $T_c$ , but the synthesis can be challenging. In this paper, we provide useful hints for the superconductor community to search for feasible MgB<sub>2</sub>-like BCS superconductors with good performance.

From a broad materials science point of view, in this paper, we demonstrate an end-to-end materials discovery strategy to forcefully filter out the desired materials via a fast and cost-effective fashion. The fourth-paradigm data-intensive scientific discovery of promising superconductors is on the radar.

## ACKNOWLEDGMENTS

Computational resources were provided by the Platform for Data-Driven Computational Materials Discovery of the Songshan Lake laboratory. We especially thank the Atomly database for data sharing. We would also acknowledge the financial support from the Chinese Academy of Sci-

ences (Grants No. XDB33010100, No. ZDBS-LY-SLH007, No. XDB33020000, No. CAS-WX2021PY-0102, and No. GJTD-2020-01), National Science Foundation of China (Grants No. 12025407 and No. 11934003), and Ministry of Science and Technology (Grants No. 2021YFA1400200 and No. 2017YFA0302903).

- [1] H. K. Onnes, Further experiments with liquid helium. C. On the change of electric resistance of pure metal's at very low temperatures etc. IV. The resistance of pure mercury at helium temperatures, Proceedings of the Royal Netherlands Academy of Arts and Sciences (KNAW) 13 II, 1274 (1911).
- [2] J. R. Gavaler, Superconductivity in Nb-Ge films above 22 K, *Appl. Phys. Lett.* **23**, 480 (1973).
- [3] J. G. Bednorz and K. A. Müller, Possible high  $T_c$  superconductivity in the Ba-La-Cu-O system, *Z. Phys. B* **64**, 189 (1986).
- [4] J. Nagamatsu, N. Nakagawa, T. Muranaka, Y. Zenitani, and J. Akimitsu, Superconductivity at 39 K in magnesium diboride, *Nature (London)* **410**, 63 (2001).
- [5] M.-K. Wu, J. R. Ashburn, C. Torng, P.-H. Hor, R. L. Meng, L. Gao, Z. J. Huang, Y. Wang, and A. Chu, Superconductivity at 93 K in a New Mixed-Phase Y-Ba-Cu-O Compound System at Ambient Pressure, *Phys. Rev. Lett.* **58**, 908 (1987).
- [6] A. P. Drozdov, M. I. Erements, I. A. Troyan, V. Ksenofontov, and S. I. Shylin, Conventional superconductivity at 203 kelvin at high pressures in the sulfur hydride system, *Nature (London)* **525**, 73 (2015).
- [7] E. Snider, N. Dasenbrock-Gammon, R. McBride, M. Debessai, H. Vindana, K. Vencatasamy, K. V. Lawler, A. Salamat, and R. P. Dias, Room-temperature superconductivity in a carbonaceous sulfur hydride, *Nature (London)* **586**, 373 (2020).
- [8] M. Tomsic, M. Rindfleisch, J. Yue, K. McFadden, J. Phillips, M. D. Sumption, M. Bhatia, S. Bohnenstiehl, and E. W. Collings, Overview of MgB<sub>2</sub> superconductor applications, *Int. J. Appl. Ceram. Technol.* **4**, 250 (2007).
- [9] D. Cunnane, K. Chen, and X. X. Xi, Superconducting MgB<sub>2</sub> rapid single flux quantum toggle flip flop circuit, *Appl. Phys. Lett.* **102**, 222601 (2013).
- [10] M. Modica, S. Angius, L. Bertora, D. Damiani, M. Marabotto, D. Nardelli, M. Perrella, M. Razeti, and M. Tassisto, Design, construction and tests of MgB<sub>2</sub> coils for the development of a cryogen free magnet, *IEEE Trans. Appl. Supercond.* **17**, 2196 (2007).
- [11] C. Poole, T. Baig, R. J. Deissler, D. Doll, M. Tomsic, and M. Martens, Numerical study on the quench propagation in a 1.5 T MgB<sub>2</sub> MRI magnet design with varied wire compositions, *Supercon. Sci. Technol.* **29**, 044003 (2016).
- [12] J. Ling, J. P. Voccio, S. Hahn, T. Qu, J. Bascuñán, and Y. Iwasa, A persistent-mode 0.5 T solid-nitrogen-cooled MgB<sub>2</sub> magnet for MRI, *Supercon. Sci. Technol.* **30**, 024011 (2016).
- [13] T. Baig, A. Al Amin, R. J. Deissler, L. Sabri, C. Poole, R. W. Brown, M. Tomsic, D. Doll, M. Rindfleisch, and X. Peng, Conceptual designs of conduction cooled MgB<sub>2</sub> magnets for 1.5 and 3.0 T full body MRI systems, *Supercon. Sci. Technol.* **30**, 043002 (2017).
- [14] D. Patel, A. Matsumoto, H. Kumakura, M. Maeda, S.-H. Kim, H. Liang, Y. Yamauchi, S. Choi, J. H. Kim, and M. S. A. Hossain, Superconducting joints using multifilament MgB<sub>2</sub> wires for MRI application, *Scr. Mater.* **204**, 114156 (2021).
- [15] Atomly, <https://atomly.net>.
- [16] A. Jain, S. P. Ong, G. Hautier, W. Chen, W. D. Richards, S. Dacek, S. Cholia, D. Gunter, D. Skinner, G. Ceder *et al.*, Commentary: The Materials Project: A materials genome approach to accelerating materials innovation, *APL Materials* **1**, 011002 (2013).
- [17] S. Curtarolo, W. Setyawan, G. L. W. Hart, M. Jahnatek, R. V. Chepulskii, R. H. Taylor, S. Wang, J. Xue, K. Yang, O. Levy *et al.*, AFLOW: An automatic framework for high-throughput materials discovery, *Comput. Mater. Sci.* **58**, 218 (2012).
- [18] J. E. Saal, S. Kirklin, M. Aykol, B. Meredig, and C. Wolverton, Materials design and discovery with high-throughput density functional theory: The Open Quantum Materials Database (OQMD), *JOM* **65**, 1501 (2013).
- [19] G. Kresse and J. Furthmüller, Efficient iterative schemes for *ab initio* total-energy calculations using a plane-wave basis set, *Phys. Rev. B* **54**, 11169 (1996).
- [20] J. P. Perdew, K. Burke, and M. Ernzerhof, Generalized Gradient Approximation Made Simple, *Phys. Rev. Lett.* **77**, 3865 (1996).
- [21] P. Giannozzi, S. Baroni, N. Bonini, M. Calandra, R. Car, C. Cavazzoni, D. Ceresoli, G. L. Chiarotti, M. Cococcioni, I. Dabo *et al.*, QUANTUM ESPRESSO: A modular and open-source software project for quantum simulations of materials, *J. Phys. Condens. Matter* **21**, 395502 (2009).
- [22] S. Baroni, S. De Gironcoli, A. Dal Corso, and P. Giannozzi, Phonons and related crystal properties from density-functional perturbation theory, *Rev. Mod. Phys.* **73**, 515 (2001).
- [23] F. Giustino, Electron-phonon interactions from first principles, *Rev. Mod. Phys.* **89**, 015003 (2017).
- [24] See Supplemental Material at <http://link.aps.org/supplemental/10.1103/PhysRevB.105.214517> for phonon spectrums, band structures, and Fermi surfaces.
- [25] P. E. Blöchl, Projector augmented-wave method, *Phys. Rev. B* **50**, 17953 (1994).
- [26] W. L. McMillan, Transition temperature of strong-coupled superconductors, *Phys. Rev.* **167**, 331 (1968).
- [27] P. B. Allen, Neutron spectroscopy of superconductors, *Phys. Rev. B* **6**, 2577 (1972).
- [28] P. B. Allen and R. C. Dynes, Transition temperature of strong-coupled superconductors reanalyzed, *Phys. Rev. B* **12**, 905 (1975).
- [29] S. Xu, C. Bao, P.-J. Guo, Y.-Y. Wang, Q.-H. Yu, L.-L. Sun, Y. Su, K. Liu, Z.-Y. Lu, and S. Zhou, Interlayer quantum transport in Dirac semimetal BaGa<sub>2</sub>, *Nat. Commun.* **11**, 2370 (2020).
- [30] S. P. Ong, W. D. Richards, A. Jain, G. Hautier, M. Kocher, S. Cholia, D. Gunter, V. L. Chevrier, K. A. Persson, and G. Ceder, Python Materials Genomics (pymatgen): A robust, open-source

- python library for materials analysis, *Comput. Mater. Sci.* **68**, 314 (2013).
- [31] S. P. Ong, L. Wang, B. Kang, and G. Ceder, Li-Fe-P-O<sub>2</sub> phase diagram from first principles calculations, *Chem. Mater.* **20**, 1798 (2008).
- [32] A. Jain, G. Hautier, S. P. Ong, C. J. Moore, C. C. Fischer, K. A. Persson, and G. Ceder, Formation enthalpies by mixing GGA and GGA + *U* calculations, *Phys. Rev. B* **84**, 045115 (2011).
- [33] M. Liu, A. Jain, Z. Rong, X. Qu, P. Canepa, R. Malik, G. Ceder, and K. A. Persson, Evaluation of sulfur spinel compounds for multivalent battery cathode applications, *Energy Environ. Sci.* **9**, 3201 (2016).
- [34] M. Aykol, S. S. Dwaraknath, W. Sun, and K. A. Persson, Thermodynamic limit for synthesis of metastable inorganic materials, *Sci. Adv.* **4**, eaaq0148 (2018).
- [35] V. A. Gasparov, N. S. Sidorov, I. I. Zver'Kova, and M. P. Kulakov, Electron transport in diborides: Observation of superconductivity in ZrB<sub>2</sub>, *JETP Lett.* **73**, 532 (2001).
- [36] D. Kaczorowski, J. Klamut, and A. Zaleski, Some comments on superconductivity in diborides, [arXiv:cond-mat/0104479](https://arxiv.org/abs/cond-mat/0104479).
- [37] N. I. Medvedeva, A. L. Ivanovskii, J. E. Medvedeva, and A. J. Freeman, Electronic structure of superconducting MgB<sub>2</sub> and related binary and ternary borides, *Phys. Rev. B* **64**, 020502(R) (2001).
- [38] P. Ravindran, P. Vajeeston, R. Vidya, A. Kjekshus, and H. Fjellvåg, Detailed electronic structure studies on superconducting MgB<sub>2</sub> and related compounds, *Phys. Rev. B* **64**, 224509 (2001).
- [39] H. Rosner, W. Pickett, S.-L. Drechsler, A. Handstein, G. Behr, G. Fuchs, K. Nenkov, K.-H. Müller, and H. Eschrig, Electronic structure and weak electron-phonon coupling in TaB<sub>2</sub>, *Phys. Rev. B* **64**, 144516 (2001).
- [40] G. Satta, G. Profeta, F. Bernardini, A. Continenza, and S. Massidda, Electronic and structural properties of superconducting MgB<sub>2</sub>, CaSi<sub>2</sub>, and related compounds, *Phys. Rev. B* **64**, 104507 (2001).
- [41] S. Elgazzar, P. M. Oppeneer, S.-L. Drechsler, R. Hayn, and H. Rosner, Calculated de Haas-van Alphen data and plasma frequencies of MgB<sub>2</sub> and TaB<sub>2</sub>, *Solid State Commun.* **121**, 99 (2002).
- [42] T. Takahashi, S. Kawamata, S. Noguchi, and T. Ishida, Superconductivity and crystal growth of NbB<sub>2</sub>, *Physica C* **426–431**, 478 (2005).
- [43] H. J. Choi, S. G. Louie, and M. L. Cohen, Prediction of superconducting properties of CaB<sub>2</sub> using anisotropic Eliashberg theory, *Phys. Rev. B* **80**, 064503 (2009).
- [44] S. Okatov, A. Ivanovskii, Y. E. Medvedeva, and N. Medvedeva, The electronic band structures of superconducting MgB<sub>2</sub> and related borides CaB<sub>2</sub>, MgB<sub>6</sub> and CaB<sub>6</sub>, *Phys. Stat. Sol. (b)* **225**, R3 (2001).
- [45] T. Oguchi, Cohesion in AlB<sub>2</sub>-type diborides: A first-principles study, *J. Phys. Soc. Jpn.* **71**, 1495 (2002).
- [46] L. Leyarovska and E. Leyarovski, A search for superconductivity below 1 K in transition metal borides, *J. Less Common Metals* **67**, 249 (1979).
- [47] A. Yamamoto, C. Takao, T. Masui, M. Izumi, and S. Tajima, High-pressure synthesis of superconducting Nb<sub>1-x</sub>B<sub>2</sub> (*x* = 0–0.48) with the maximum *T<sub>c</sub>* = 9.2 K, *Physica C* **383**, 197 (2002).
- [48] H. Takeya, K. Togano, Y. S. Sung, T. Mochiku, and K. Hirata, Metastable superconductivity in niobium diborides, *Physica C* **408**, 144 (2004).
- [49] J. K. Hulm and B. T. Matthias, New superconducting borides and nitrides, *Phys. Rev.* **82**, 273 (1951).
- [50] W. T. Ziegler and R. A. Young, Studies of compounds for superconductivity, *Phys. Rev.* **90**, 115 (1953).
- [51] J. Schirber, D. Overmyer, B. Morosin, E. Venturini, R. Baughman, D. Emin, H. Klesnar, and T. Aselage, Pressure dependence of the superconducting transition temperature in single-crystal NbB<sub>x</sub> (*x* near 2) with *T<sub>c</sub>* = 9.4 K, *Phys. Rev. B* **45**, 10787 (1992).
- [52] H. Kotegawa, K. Ishida, Y. Kitaoka, T. Muranaka, N. Nakagawa, H. Takagiwa, and J. Akimitsu, Evidence for strong-coupling *s*-wave superconductivity in MgB<sub>2</sub>: <sup>11</sup>B-NMR study of MgB<sub>2</sub> and the related materials, *Physica C* **378–381**, 25 (2002).
- [53] D. Kaczorowski, A. Zaleski, O. Żogał, and J. Klamut, Incipient superconductivity in TaB<sub>2</sub>, [arXiv:cond-mat/0103571](https://arxiv.org/abs/cond-mat/0103571).
- [54] S. Sanfilippo, H. Elsinger, M. Nunez-Regueiro, O. Laborde, S. LeFloch, M. Affronte, G. Olcese, and A. Palenzona, Superconducting high pressure CaSi<sub>2</sub> phase with *T<sub>c</sub>* up to 14 K, *Phys. Rev. B* **61**, R3800 (2000).
- [55] S. Gabani, K. Flachbart, K. Siemensmeyer, and T. Mori, Magnetism and superconductivity of rare earth borides, *J. Alloys Compd.* **821**, 153201 (2020).
- [56] C. Parlak, The physical properties of AlB<sub>2</sub>-type structures CaGa<sub>2</sub> and BaGa<sub>2</sub>: An *ab-initio* study, *Physica B* **576**, 411724 (2020).
- [57] B. Song, Y. Zhou, H. M. Yang, J. H. Liao, L. M. Yang, X. B. Yang, and E. Ganz, Two-dimensional anti-Van't Hoff/Le Bel array AlB<sub>6</sub> with high stability, unique motif, triple Dirac cones, and superconductivity, *J. Am. Chem. Soc.* **141**, 3630 (2019).
- [58] G. Huang, M. Liu, L. F. Chen, and D. Y. Xing, First-principles calculation of superconductivity in pseudo-ternary silicides *M*GaSi (*M* = Ca, Sr and Ba), *Physica C* **423**, 9 (2005).
- [59] E. Baldini, A. Mann, L. Benfatto, E. Cappelluti, A. Acocella, V. M. Silkin, S. V. Ereemeev, A. B. Kuzmenko, S. Borroni, and T. Tan, Real-Time Observation of Phonon-Mediated  $\sigma$ - $\pi$  Interband Scattering in MgB<sub>2</sub>, *Phys. Rev. Lett.* **119**, 097002 (2017).
- [60] D. Novko, F. Caruso, C. Draxl, and E. Cappelluti, Ultrafast Hot Phonon Dynamics in MgB<sub>2</sub> Driven by Anisotropic Electron-Phonon Coupling, *Phys. Rev. Lett.* **124**, 077001 (2020).
- [61] E. Cappelluti, F. Caruso, and D. Novko, Properties and challenges of hot-phonon physics in metals: MgB<sub>2</sub> and other compounds, *Prog. Surf. Sci.* **100664** (2022), doi: [10.1016/j.progsurf.2022.100664](https://doi.org/10.1016/j.progsurf.2022.100664).
- [62] E. Cappelluti and D. Novko, Fingerprints of hot-phonon physics in time-resolved correlated quantum lattice dynamics, *SciPost Phys.* **12**, 173 (2022).
- [63] F. Bouquet, R. Fisher, N. Phillips, D. Hinks, and J. Jorgensen, Specific Heat of Mg<sup>11</sup>B<sub>2</sub>: Evidence for a Second Energy Gap, *Phys. Rev. Lett.* **87**, 047001 (2001).
- [64] K.-P. Bohnen, R. Heid, and B. Renker, Phonon Dispersion and Electron-Phonon Coupling in MgB<sub>2</sub> and AlB<sub>2</sub>, *Phys. Rev. Lett.* **86**, 5771 (2001).

- [65] G. V. Samsonov, *Handbook of Refractory Compounds* (Springer, New York, 1980).
- [66] S. M. Sichkar and V. N. Antonov, Electronic structure, phonon spectra and electron-phonon interaction in ScB<sub>2</sub>, *Low Temp. Phys.* **39**, 595 (2013).
- [67] A. S. Cooper, E. Corenzwit, L. D. Longinotti, B. T. Matthias, and W. H. Zachariasen, Superconductivity: The transition temperature peak below four electrons per atom, *Proc. Natl. Acad. Sci.* **67**, 313 (1970).